Theoretical Notes
Note 216

TN 216

DNA 3455T

ANALYSIS OF THE RESPONSE OF A CONDUCTOR IMMERSED IN AN EMP SOURCE REGION-THE STEADY STATE

R & D Associates
Box 3580
Santa Monica, California 90403

Charles T. C. Mo

24 January 1975

Topical Report

CONTRACT No. DNA 001-72-C-0197

THIS WORK SPONSORED BY THE DEFENSE NUCLEAR AGENCY
UNDER SUBTASK DB001-10.

Prepared for

Director
DEFENSE NUCLEAR AGENCY
Washington, D. C. 20305

PREFACE

Helpful discussions with Drs. W. R. Graham and W. J. Karzas, and Mr. R. R. Schaefer during the course of this work are acknowledged by the author.

TABLE OF CONTENTS

SECTION 1

INTRODUCTION TO THE SOURCE REGION PROBLEM

1.1 INTRODUCTION

It is well known [1-3] that in a nuclear detonation the γ-rays generated by fission and various nuclear scatterings and the x-rays generated by the heated bomb materials can scatter electrons in the weapon and the surrounding materials. These electrons constitute a current which, if asymmetrically distributed and/or gyrating in a magnetic field, can coherently radiate an electromagnetic pulse (EMP) of microwave frequency or lower. This EMP can propagate much further than the γ-rays or the x-rays that create it, and can couple into a system or a device at great distances. The EMP effects depend, of course, on the location of the burst (such as high altitude, air, surface, underground or underwater), the detonation material and materials in its vicinity, the media along the γ-ray or x-ray paths, the presence of a biasing magnetic field, and the location of the observer.

To calculate the generation of the EMP, we need to estimate the photon spectral flux from the burst, the different species and densities of materials present, and various electrodynamic interaction cross sections. A macroscopic model for the source current and the environmental medium can be constructed from these quantities, and then classical EM theory governs the generation, propagation, and coupling of the EMP. For objects outside of the source region the processes of propagation and coupling can be addressed independently [4].

However, if a system of interest (such as a missile or a satellite) is located in the region where the source current generating mechanism is present, then the EMP generation and coupling phenomena are combined and must be analyzed together.

In this report, we examine the problem of a conductor immersed in an EMP source region at steady-state. This steady-state case is applicable when the γ-flux illumination changes slowly and lasts a long time, the conductor is small, and the skin depth of the source region environment is large. It illustrates the physical process involved and may provide an upper bound limit to the time-dependent case. Typical numerical data considered are for high altitude EMP threat exposures.

Essentially, the steady-state solution describes the effect on a conductor that sees and responds to the instantaneous environment as a whole. The other extreme case of a very short skin depth, which shields one part of the conductor from the other part, and its time-dependent local effects are treated in a separate report [5].

1.2 THE PHYSICS OF THE PROBLEM

Consider a conducting body at a height $h \gtrsim 20$ km from the earth surface which is illuminated by the photon-flux from a high-altitude nuclear burst at 100 km or above. Now the x-rays of $\sim$ keV energy in the detonation radiation are absorbed in the surrounding materials predominantly by the photoelectric interaction, with a mass attenuation coefficient $\mu_x/\rho \equiv NZ\sigma_x/\rho \sim 4.5$ cm^2/gm [6]

in air for 10 keV x-rays. Here $N \equiv$ # density of atoms in air, $Z \equiv$ average atomic number for air species, $\sigma_x \equiv$ photoelectric absorption cross section, and $\rho \equiv$ density of air. Also the γ-rays are attenuated predominantly by the Compton scattering with $\mu_\gamma/\rho \equiv NZ\sigma_\gamma/\rho \sim 2.6 \times 10^{-2}$ cm^2/gm in air for ~ 1 meV γ-rays.

Thus the $\sim$1 meV γ-rays, with an attenuation mean free path $\lambda_{\gamma\text{-air}}$ approximately 173 times of the attenuation mean free path $\lambda_{x\text{-air}}$ for the $\sim$10 keV x-rays, become the dominant flux if the air content between the burst and the region of interest exceeds $(\rho/\mu_x)\ell n(90/0.03) \sim 1.78$ gm/cm^2. Here we assume that the x-rays and γ-rays respectively have 70 percent and 0.03 percent of the original yield [7]. This assumption is satisfied if the region of interest has a height $h \leq 44$ km, the case under consideration. We therefore can concentrate only on the effect of γ-rays.

Now consider a conducting body of length L and cross sectional width D at $h \sim 40$ km in an EMP source region, with dimensions on the order of $D \sim 1$ meter and $L \sim 10$ meters (see Figure 1). A 1 meV γ-ray has a Compton absorption mean free path $\lambda_{\gamma\text{-air}} \equiv (\mu_{\gamma\text{-air}})^{-1} \sim 9.6 \times 10^4$ meter in the air with a density $\sim 4 \times 10^{-6}$ gm/cm^3 at $\sim$40 km. Also the mean free paths for aluminum and lead are $\lambda_{\gamma\text{-A}\ell} \sim 0.14$ meter and $\lambda_{\gamma\text{-Pb}} \sim 0.038$ meter, respectively, and hence

$$\lambda_{\gamma\text{-air}} \gg L,\ D \gg \lambda_{\gamma\text{-conductor}} \qquad (1\text{-}1)$$

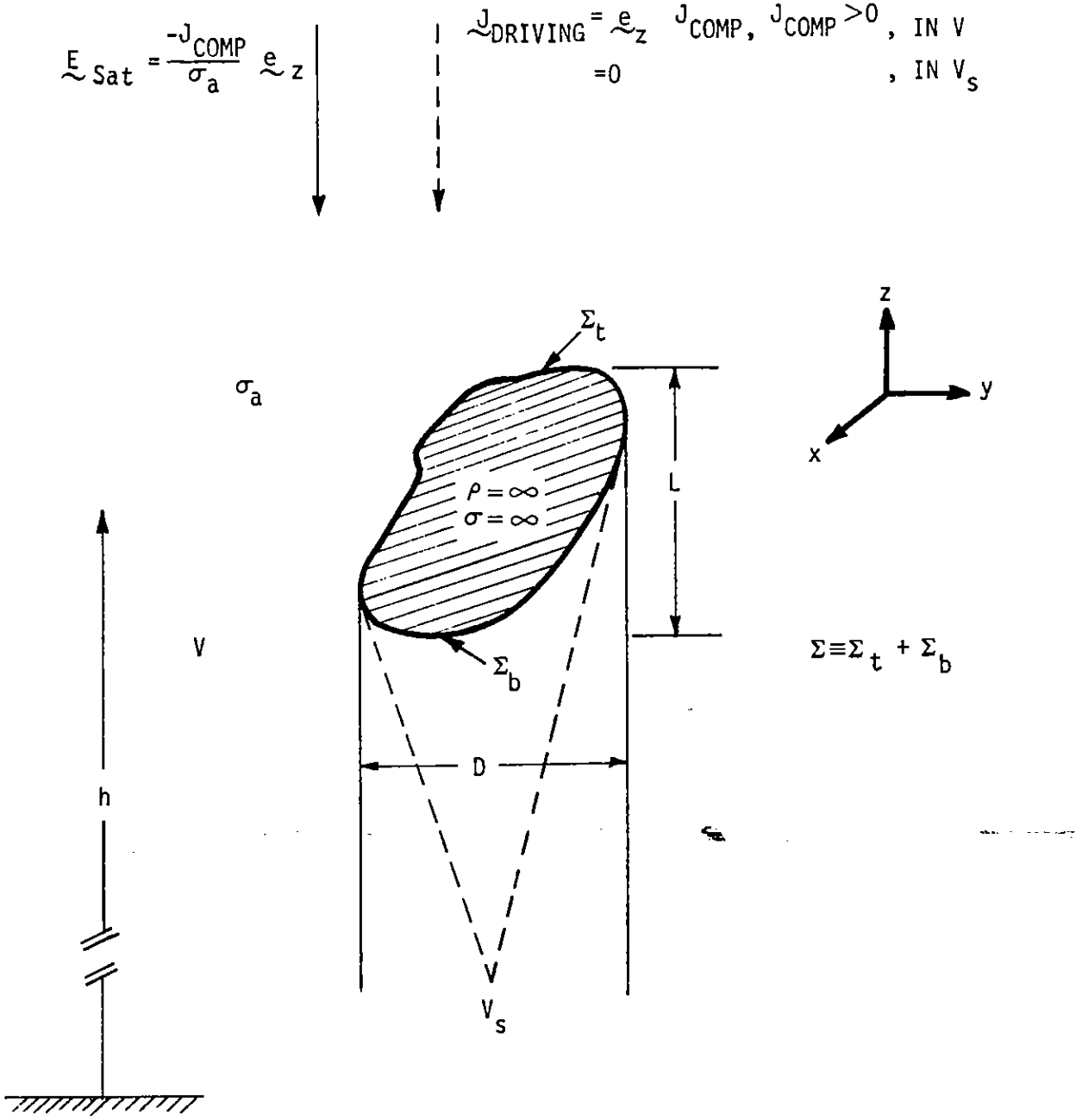

Figure 1. A Conductor Immersed in EMP Source Region

in the analysis. For simplicity, we thus can assume that the conductor has a large density such that $\lambda_{\gamma\text{-conductor}} = 0$, and the γ-rays do not penetrate any depth into the conductor. Also the first inequality in (1-1) enables us to assume the γ-flux to be spatially uniform (except in the shadow region V_s where it is zero) for the problem considered. Notice that the γ-thickness in most situations does hold, but its being all due to the conducting surface is an idealization.

To describe the incident field and current without the presence of the conductor, first the γ-flux creates a convection current by Compton scattering. Also, an ionization air conductivity σ_a [8] is produced by the inelastic Coulomb scatterings between the Compton electrons and the air, at the average expense of 32 eV/ion-pair from the Compton electron's kinetic energy [9]. The current is [10, 11]

$$J_{comp} = eF_\gamma \cdot \frac{R_{mf}}{\lambda_\gamma} \sim eF_\gamma \times 2.5 \times 10^{-3} \text{ amp} \qquad (1\text{-}2)$$

where $F_\gamma \equiv$ number flux of γ-rays in $1/(m^2 - sec)$, and $R_{mf} \equiv$ mean forward range of electrons ($\sim$0.079 gm/cm^2 for $\sim$0.45 meV average Compton electrons) $\sim$200 meters in air at h $\sim$ 40 km. The electron air conductivity [12] is typically

$$\sigma_a \sim 3.4 \times 10^{-8} \eta_e \text{ mho/meter} \qquad (1\text{-}3)$$

where η_e = electron number density in $1/(\text{meter}^3)$. Also a typical prompt gamma flux F_γ is, assuming the 1 meV γ-rays isotopically emitted claiming ~0.03 percent of yield [13],

$$F_\gamma = \frac{\Gamma}{4\pi r^2} \cdot \frac{e^{\alpha t}}{e^{3\alpha t/2} + 1} \; e^{-\int \frac{dr}{\lambda_\gamma}} \qquad (\text{meter}^2 - \text{sec})^{-1} \qquad (1\text{-}4a)$$

where

$$\begin{aligned} &\alpha \sim 10^8 \text{ sec}^{-1} \\ &\Gamma = 4.51 \times 10^{21} \alpha Y \\ &Y \equiv \text{yield in kilotons} \\ &r \equiv \text{distance in meters from the burst point} \end{aligned} \qquad (1\text{-}4b)$$

Now, the problem is, what are the electromagnetic responses of a conductor if it is immersed in a source region as described above? Especially of interest are the total charge and surface charge density, the electric field, the magnetic field, and the current and its density on the surface of the conductor. We analyze the steady-state situation in Section 2, solve such a steady state for a prolate spheroid in Section 3, outline the formulation for the time-dependent case in Section 4.1, and summarize the conclusions briefly in Section 4.2.

SECTION 2

STEADY-STATE ANALYSIS

2.1 GENERAL REMARKS

Interesting EMP source region interactions are, of course, time dependent. The motivations for looking into a steady-state solution are

1. to illuminate the physical processes involved;
2. to provide possible limiting estimates for the time-dependent solutions; and
3. to establish a method of analysis which may be extended into the dependent case (e.g., Helmhotz eq. instead of Laplace eq.).

Now the wavelength of the ~1 meV γ-rays ($\sim 1.24 \times 10^{-12}$ meter) is much shorter than the dimension of the conductor concerned, the γ-flux F_γ, and its accompanying primary Compton current can be taken to be zero in the geometrical shadow region V_s (see Fig. 1) as a result of $\rho = \infty$ from condition (1-1). Also from (1-1), F_γ and J_{comp} can be assumed to be uniform in V. Further, ignoring the ρ_{air} variation (the scale height at 40 km is ~ 7 km >> L, D) makes σ_a in the steady-state to be uniform in V. But in V_s we cannot assume zero conductivity, although there are no primary γ-rays in V_s. This is because (1) the Klein-Nishina differential cross section gives the primary Compton electrons a forward angular spread $\Delta_\theta \sim 30^\circ$ for the 1 meV γ-rays, and (2) the ionized particles are diffused into V_s. Mechanism (1) limits the part in V_s with conductivity appreciably different from the uniform σ_a to

$$|\Delta z| \lesssim D \cot 15^{\circ} = 3.7\ D \qquad (2\text{-}1)$$

from the bottom of the conductor's surface Σ_b (see Figure 1). Since in mechanism (2) the electron attachment is much faster than the electron-ion and ion-ion recombinations, the ion recombination mean free path is roughly

$$\lambda_{recomb} \sim \frac{v_t}{k_3 N_i} \sim 0.2 \text{ meter} \qquad (2\text{-}2)$$

where the ion-thermal velocity $v_t \sim \sqrt{8kT/\pi m_i} \sim 4.3 \times 10^2$ meter/sec, $T \sim 273^{\circ}K$, $k_3 \sim 2 \times 10^{-12}$ m^3/sec [14], and $N_i \sim 10^{18}\ (\rho_{air}/\rho_o) \sim 10^{15}/meter^3$ are used. Therefore the low conductivity region of (2-1) is further reduced by the inward diffusion erosion (2-2). We thus assume σ_a to be uniform everywhere in V and V_s. That the error of such an approximation depends on the "slenderness" of the conductor will be shown in Section 2.6. Finally we notice that the assumption of $J_{comp} = 0$ but $\sigma_a \neq 0$ in V_s is not inconsistent, because the J_{comp} in V_s (1) has no direct charge deposition effect and (2) has its indirect field effect being accounted for by a charge separation field $\underset{\sim}{E}_p$ everywhere.

2.2 STEADY-STATE CRITERION FOR γ-FLUX AND GEOMETRY

The steady-state behavior will really be achieved if γ-flux duration satisfies

$$\tau_\gamma \gg \tau_{body},\ \tau_{rad},\ \tau_{built} \equiv \frac{\varepsilon}{\sigma_a} \qquad (2\text{-}3)$$

where $\tau_{body} = L/c$ is time for a surface signal to travel from end to end on the conductor, $c \equiv$ vacuum velocity of light, $\tau_{rad} \equiv$ typical time needed for the conductor in some initial charge distribution to reach its equilibrium charge distribution by radiation, and $\tau_{built} \equiv$ typical build-up time for the charge separation parallel to field to reach its saturated value J_{comp}/σ_a.

We can roughly estimate τ_{rad} by

$$\tau_{rad} \sim \frac{\mathcal{E}_i - \mathcal{E}_f}{P_{rad}} \tag{2-4}$$

where

$\mathcal{E}_i$, $\mathcal{E}_f \equiv$ initial, final electrostatic energy of the respective charge configurations, and

$P_{rad} \equiv$ power radiated by the conductor when it is redistributing its surface charges into equilibrium.

We will find that the τ_{built} is also the typical time needed for the conductor to accrue its equilibrium charge (see eq. (2-13)).

The condition (2-3) dictates physical situations in which the steady-state results directly apply. Essentially the condition requires a small conductor and a long-duration γ-flux (such as might be provided by delayed or secondary γ-rays).

2.3 SEPARATION INTO TWO BASIC EFFECTS

The electromagnetic effects of the γ-rays on the conductor are determined completely by the driving current $\underset{\sim}{J}_{driving}$ [15] and the charge separation field $\underset{\sim}{E}_{sat}$, except the direct deposit of γ-rays on the conductor. This direct deposit of the γ-rays only dissipates into heat near the front conductor surface, through Compton scattering and successive multiple Coulomb collisions (ignore the backscattered electrons leaving the conductor), and does not produce current or electric field because of the $\rho = \infty$ and $\sigma = \infty$ condition for the conductor. With the approximation σ_a = constant, the effects of $\underset{\sim}{J}_{driving}$ and $\underset{\sim}{E}_{sat}$ can be separated into the following aspects:

1. The Compton electrons of the $\underset{\sim}{J}_{comp}$ (1-2) collide with the conductor's front surface and essentially are stopped in a thin layer near that surface because of the high density of the conductor (e.g., $R_{mf} \sim 1.6 \times 10^{-4}$ meter for conductor density of ~ 5 gm/cm^3 and for ~ 0.45 meV electrons). The conductor thus receives a net deposited charge.

2. The driving Compton current gives rise to an induced parallel electric field $\underset{\sim}{E}_p$ due to charge separation. The $\underset{\sim}{E}_p = E_p \underset{\sim}{e}_z$ is

limited by the air conductivity's backflowing air conduction current and builds up according to

$$-\frac{\partial}{\partial t}(\epsilon E_p) = J_{Comp} + \sigma_a E_p$$

$$\Longrightarrow E_p(t) = \frac{-J_{Comp}}{\sigma_a}\left(1 - e^{\frac{-\sigma_a t}{\epsilon}}\right) \xrightarrow[t \gg \frac{\epsilon}{\sigma_a}]{} \frac{-J_{Comp}}{\sigma_a} \equiv E_{sat} \qquad (2\text{-}5)$$

where ϵ = dielectric constant of the air and is $\approx \epsilon_o$ of the vacuum. The conductor is immersed in this external parallel electric field $\underset{\sim}{E}_{sat}$. That the external saturated field is $-J_{Comp}/\sigma_a$ and constant everywhere, even in the shadow region V_s, is really justified by its physical origination: it is caused by charge separation layers at large distances from the conductor and large in their horizontal sizes compared with the conductor.

The separation into these two effects (see also Section 2.4) enables us to view the overall steady-state situation in a simple way. The perfect conductor, immersed in an external field $\underset{\sim}{E}_{sat}$, maintains on its surface an induced surface charge distribution ρ_1 which is a balance between the conduction loss rate $\sigma_a \underset{\sim}{E}_1$ caused by the surrounding air conductivity σ_a and the polarizing influence of $\underset{\sim}{E}_{sat}$. This balance provides a surface current density $\underset{\sim}{K}_1$. Also, the total amount of charge $\oint_\Sigma \rho_2 da$ deposited by the Compton current on the conductor is released by the balance of another air conductivity current $\sigma_a \underset{\sim}{E}_2$,

where $\underset{\sim}{E}_2$ is the static field caused by the net charge deposition. This balance also gives rise to a surface current $\underset{\sim}{K}_2$ (see Fig. 4 on p. 26). The superposition of these two effects gives the total electrostatic field, surface charge and current density. Then the time-independent current distributions determine the magnetostatic field.

Before going into detail, we must emphasize that the conductivity σ_a does not alter any electrostatics, except by requiring a "driving source" to maintain the static charge and current configurations, if and only if,

$$\underset{\sim}{\nabla}\, \sigma_a \cdot \underset{\sim}{E} = 0 \qquad (2\text{-}6)$$

is satisfied. Here $\underset{\sim}{E}$ is the static electric field <u>before</u> σ_a is introduced. Eq. (2-6) simply guarantees no new spatial accumulation of charges by the introduction of the conductivity σ_a. Physically, the σ_a introduced should be constant along the $\underset{\sim}{E}$ field lines. Trivially, the approximation σ_a = constant in V and V_s satisfies (2-6).

We label the quantities associated with the parallel saturated field $\underset{\sim}{E}_{sat}$ by the subscript 1, and the quantities associated with the net charge deposition by the subscript 2 in the following analysis.

2.4 THE ELECTROSTATIC FIELD

From Maxwell eqs., the total electrostatic field $\underset{\sim}{E}$ satisfies

$$\underset{\sim}{E} \equiv \underset{\sim}{E}_1 + \underset{\sim}{E}_2 = -\nabla \Phi_1 - \nabla \Phi_2 \tag{2-7}$$

where $\underset{\sim}{E}_1$, the effect of the parallel field $\underset{\sim}{E}_{sat}$, obeys

$$\begin{cases} \nabla^2 \Phi_1 = 0 \quad \text{in } V \text{ and } V_s \\ \Phi_1 = 0 \quad \text{on } \Sigma \\ \Phi_1 \longrightarrow -E_{sat} \cdot z \quad \text{as } r \to \infty \end{cases} \tag{2-8}$$

and $\underset{\sim}{E}_2$, the effect of the charge deposited by $\underset{\sim}{J}_{Comp}$, obeys

$$\begin{cases} \nabla^2 \Phi_2 = 0 \quad \text{in } V \text{ and } V_s \\ \Phi_2 = \text{Const. on } \Sigma \\ \Phi_2 \longrightarrow \dfrac{Q_{total}}{4\pi\epsilon r} + 0\left(\dfrac{1}{r^2}\right) \quad \text{as } r \to \infty . \end{cases} \tag{2-9}$$

Here Σ is the conductor's surface, and $O(1/r^2)$ represents a quantity whose ratio to $(1/r^2)$ is finite as $r \to \infty$.

The total charge Q_{total} on the conductor is determined by the charge conservation

$$\oint_{\Sigma} \underset{\sim}{J} \cdot d\underset{\sim}{a} = \oint_{\Sigma_\infty} \underset{\sim}{J} \cdot d\underset{\sim}{a} = 0 \tag{2-10}$$

where $\Sigma_\infty \equiv$ a closed surface at $r = \infty$ and

$$\underset{\sim}{J} = \sigma_a \underset{\sim}{E} + \underset{\sim}{J}_{driving} \tag{2-11}$$

From (2-10) and (2-11), we immediately have

$$Q_{total} = \frac{\epsilon}{\sigma_a} \int_{\Sigma_t} \underset{\sim}{J}_{Comp} \cdot d\underset{\sim}{a}. \tag{2-12}$$

Notice that the total charge on Σ is determined only by the $\underset{\sim}{J}_{Comp}$ and σ_a, but not by the parallel $\underset{\sim}{E}_{sat}$ which induces no net charge on the conductor. Here Σ_t is the top illuminated part of Σ.

2.5 THE MAGNETOSTATICS

The current density $\underset{\sim}{J}$ and surface current density $\underset{\sim}{K}_s$ obtained in the electrostatics determine the magnetostatic field $\underset{\sim}{B}$, except $\underset{\sim}{B}$ influences the air conducting current through [16]

$$\underset{\sim}{J}_{\text{cond. air}} = \sum_i \frac{\sigma_i \left\{ \underset{\sim}{E} + \frac{\tau_i}{m_i} e_i \left[\underset{\sim}{E} \times \underset{\sim}{B} + \frac{\tau_i}{m_i} e_i \, \underset{\sim}{E} \cdot \underset{\sim}{B} \, \underset{\sim}{B} \right] \right\}}{1 + \left(B \frac{\tau_i \, e_i}{m_i} \right)^2} \qquad (2\text{-}13)$$

where $\sigma_i \equiv$ electric conductivity without magnetic field, $\tau_i \equiv$ mean collision time, $m_i \equiv$ mass, $e_i \equiv$ charge of the i^{th} charge species in the ionized air.

So if

$$\frac{B\tau e}{m} \ll 1 \text{ or } \nu_B \equiv \frac{eB}{m} \ll \frac{1}{\tau} \equiv \nu_C \qquad (2\text{-}14)$$

where $\nu_B \equiv$ gyration frequency in B and $\nu_C \equiv$ collision frequency of the ionized charge species, we can ignore the influence of B on σ_a and maintain σ_a = constant as if no conductor exists. In fact this assumption

has already been used in that the induced E does not change the incident air conductivity. This assumption makes the present analysis a first-order linear model.

Within the above accuracy, the magnetic field is determined by the currents by

$$\begin{cases} \nabla^2 \underset{\sim}{B} = -\mu \nabla \times \underset{\sim}{J}_{\text{driving}} & \text{in V and } V_s \\ \underset{\sim}{n} \times \underset{\sim}{B} = \mu \underset{\sim}{K}_s & \text{on } \Sigma. \end{cases} \tag{2-15}$$

Notice that the only contributing volume current is the "shadow Compton Current". This shadow current flows in the shadow region V_s just to cancel the Compton current which would have been there if no conductor were present (see Fig. 1)[17].

The surface current density $\underset{\sim}{K}_s$ on Σ is determined by the surface charge conservation in steady state

$$\nabla_{(2)} \cdot \underset{\sim}{K}_s = -\underset{\sim}{J} \cdot \underset{\sim}{n} - \frac{\partial \rho_s}{\partial t} \quad \text{on } \Sigma \tag{2-16}$$

where $\rho_s \equiv$ surface charge density and $\nabla_{(2)}$ is the two-dimensional del operator on Σ (notice $\nabla_{(2)}$ differs from the 2-dimensional-part of the 3-dimensional ∇)[18]. Also notice that (2-10) and (2-16) imply

$$\oint_{\Sigma_1} \underset{\sim}{K} \cdot d\underset{\sim}{\ell}_n + \oint_{\Sigma_2} \underset{\sim}{K} \cdot d\underset{\sim}{\ell}_n = 0 \tag{2-17}$$

where Σ has been divided in two arbitrary parts, Σ_1 and Σ_2, and $d\underset{\sim}{\ell}_n \equiv \underset{\sim}{n} \times d\underset{\sim}{\ell}$ with $d\underset{\sim}{\ell} \equiv$ enclosing line segment of Σ_1 or Σ_2.

2.6 INHOMOGENEOUS CONDUCTIVITY

The effect of inhomogeneity in air conductivity would be to pile up certain space charges to the constant σ_a solution at the places where $\underset{\sim}{\nabla}\sigma_a \cdot E \neq 0$.

If the conductor is thin, i.e., the cross-sectional area of the shadow is small compared to the total surface area, then the inhomogeneity of conductivity has a small effect on the total field and can be treated by perturbation. Such a small perturbing space charge is

$$\rho_{sp} = \frac{-\epsilon \underset{\sim}{E} \cdot \underset{\sim}{\nabla}\sigma_a}{\sigma_a} \tag{2-18}$$

where $\underset{\sim}{E}$ is the unperturbed field of uniform σ_a. The total perturbing spatial charge is

$$q_{sp} = \int \rho_{sp}\, d^3x \sim -\epsilon\,(EA)_{\text{shadow, near } \Sigma_b} \sim Q_{\text{bottom}} \tag{2-19}$$

Thus the q_{sp}, located in V_s near Σ_b, is $\sim Q_{\text{bottom}}$ as expected. The rough error estimate for the whole solution is thus $\sim Q_{\text{bottom}}/Q_{\text{total}} \sim (\Sigma_b/\Sigma)^{1/2}$.

This justifies the validity of the approximation for a "thin" or "slender" conductor.

If the conductor is not thin, or $\sigma_a(X)$ is badly inhomogeneous, we should re-solve the whole steady-state problem replacing the Laplace eqs. in (2-8) and (2-9) by

$$\nabla^2 \Phi + \frac{\nabla\sigma \cdot \nabla\Phi}{\sigma} = 0 \qquad (2\text{-}20)$$

and keeping other requirements as before (of course still with $\sigma_a \longrightarrow$ uniform as $r \rightarrow \infty$).

SECTION 3

A PROLATE SPHEROIDAL CONDUCTOR IN STEADY-STATE

3.1 GENERAL REMARKS

If the conductor's surface coincides with one of the eleven separable coordinate systems for the Laplace equation, the electrostatics can be solved easily. Otherwise, special techniques have to be employed for different problems. In the following we solve the problem of a prolate spheroid conductor immersed in a source region with its axis parallel and perpendicular to the incident γ-flux.

3.2 PARALLEL TO γ-FLUX ILLUMINATION

Referring to Figure 2, consider a prolate spheroidal conductor with its axis being the z-axis and parallel to the γ-flux incidence as illustrated. In a prolate spheroidal coordinate system (η, θ, ϕ)[19] with infinitesimal length

$$ds^2 = \ell^2(\sinh^2\eta + \sin^2\theta)\left[(d\eta)^2 + (d\theta)^2\right] + \ell^2 \sinh^2\eta \sin^2\theta (d\phi)^2 \quad (3\text{-}1)$$

where $0 \leq \eta \leq \infty$, $0 \leq \theta \leq \pi$, and $0 \leq \phi \leq 2\pi$,

the conductor's surface Σ is described by

$$\eta = \eta_o. \quad (3\text{-}2)$$

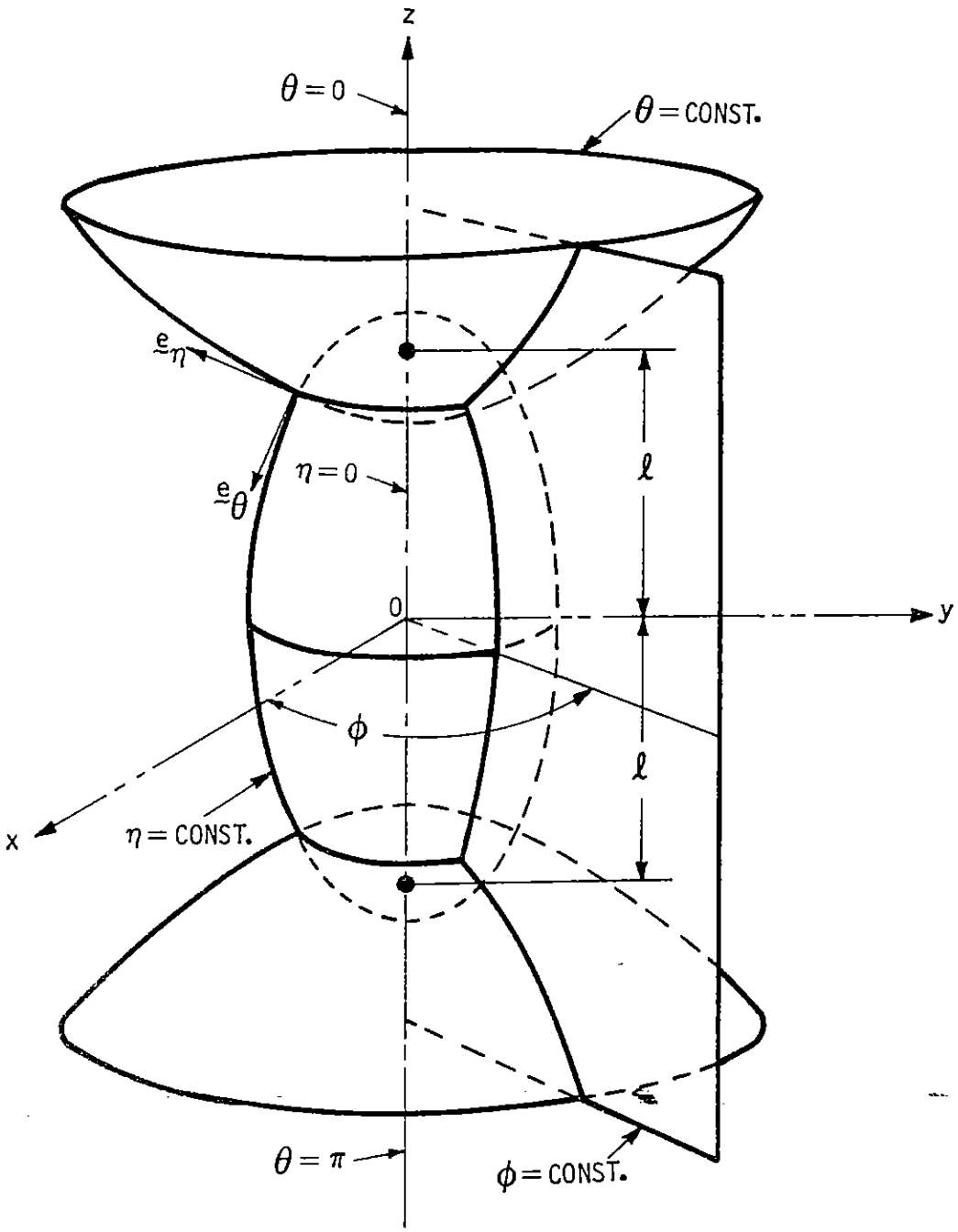

Figure 2. A Prolate Spheroidal Conductor Parallel to γ - Flux Illumination

The dimension of the conducting spheroid is

$$L = 2\ell \cosh \eta_o$$

$$D = 2\ell \sinh \eta_o \tag{3-3}$$

with the ratio of diameter to length

$$\frac{D}{L} = \tanh \eta_o. \tag{3-4}$$

With the ϕ-independent symmetry, the general potential Φ is

$$\Phi = \sum_0^\infty P_n(\cos \theta) \left[a_n P_n(\cosh \eta) + \beta_n Q_n(\cosh \eta)\right] \tag{3-5}$$

where $P_n(X)$ and $Q_n(X)$ are respectively Lengendre polynomials of first and second kind, and a_n, β_n are arbitrary constants.

3.2.1 The Electrostatic Field $\underset{\sim}{E}_1$ Caused by $\underset{\sim}{E}_{sat}$

Imposing the boundary requirement (2-8) on (3-5), the potential Φ_1 and electrostatic field $\underset{\sim}{E}_1$ caused by the parallel saturated field $\underset{\sim}{E}_{sat}$ are

$$\Phi_1(\eta, \theta) = \frac{j_{comp}\ell}{\sigma_a} \left[\cosh \eta - \frac{\cosh \eta_o}{Q_1(\cosh \eta_o)} Q_1(\cosh \eta)\right] \cos \theta \tag{3-6}$$

$$\underset{\sim}{E}_1(\eta, \theta) = \frac{-J_{comp}}{\sigma_a} \underset{\sim}{e}_z + \frac{J_{comp}}{\sigma_a} \frac{\cosh \eta_o}{Q_1(\cosh \eta_o) \left[\sinh^2 \eta_o + \sin^2\theta\right]^{1/2}}$$

$$\left\{\underset{\sim}{e}_\eta \sinh \eta \, Q_1'(\cosh \eta) \cos\theta - \underset{\sim}{e}_\theta \sin\theta \, Q_1(\cosh \eta)\right\} \qquad (3\text{-}7)$$

where the $Q_1(\xi) \equiv (\xi/2) \ln \left[(\xi + 1)/(\xi - 1)\right] - 1 \to (3\xi^2)^{-1}$ as $\xi \to \infty$. That there is no net charge on $\eta = \eta_o$ associated with this $\underset{\sim}{E}_1$ can be seen easily from either $\int_{\eta_o} \underset{\sim}{E}_1 \cdot d\underset{\sim}{a} = 0$ or the induced potential (the second term of (3-6)) $\to r^{-2}$ as $r = \ell(\cosh^2\eta - \sin^2\theta)^{1/2} \to \infty$. Also we rewrite $\underset{\sim}{E}_1$ as [20]

$$\underset{\sim}{E}_1 = \frac{-J_{comp}}{\sigma_a(\sinh^2\eta + \sin^2\theta)^{1/2}} \left\{\underset{\sim}{e}_\eta \cos\theta \sinh \eta\left[1 - \frac{\cosh \eta_o \, Q_1'(\cosh \eta)}{Q_1(\cosh \eta_o)}\right]\right.$$

(3-8)

$$\left. -\underset{\sim}{e}_\theta \sin\theta \left[\cosh \eta - \frac{\cosh \eta_o \, Q_1(\cosh \eta)}{Q_1(\cosh \eta_o)}\right]\right\}$$

to reveal more clearly its surface charge density which is $\epsilon \underset{\sim}{E}_1 \underset{\sim}{e}_\eta$ at $\eta = \eta_o$.

3.2.2 The Electrostatic Field $\underset{\sim}{E}_2$ Caused by the Charge Deposition of $\underset{\sim}{J}_{comp}$

Using (2-9) in (3-5), we obtain

$$\Phi_2 = \frac{-\ell \sinh^2 \eta_o}{4\sigma_a} \cdot J_{comp} \cdot Q_o(\cosh \eta) \qquad (3\text{-}9)$$

$$\underset{\sim}{E}_2 = \frac{-\sinh^2 \eta_o}{4\sigma_a} \cdot J_{comp} \cdot \frac{e_\eta}{\sinh \eta \cdot \left[\sinh^2 \eta + \sin^2 \theta \right]^{1/2}} \qquad (3\text{-}10)$$

where $Q_o(\xi) \equiv (1/2)\, \ell n \left[(\xi + 1)/(\xi - 1) \right] \rightarrow \xi^{-1}$ as $\xi \rightarrow \infty$, and we have made use of (2-12) to relate Q_{total} to J_{comp} by

$$Q_{total} = \frac{-\epsilon}{\sigma_a} J_{comp} (\ell \sinh \eta_o)^2 \pi. \qquad (3\text{-}11)$$

Incidentally, (3-11) together with (3-9) gives the capacitance of the spheroid

$$C = \frac{4\pi \epsilon \ell}{Q_o(\cosh \eta_o)} \cdot \qquad (3\text{-}12)$$

3.2.3 The Total Electrostatic Field $\underset{\sim}{E}$ and Charge Density

Superimposing $\underset{\sim}{E}_1$ and $\underset{\sim}{E}_2$, the total $\underset{\sim}{E}$ is just

$$\underset{\sim}{E} \equiv E_\eta \underset{\sim}{e}_\eta + E_\theta \underset{\sim}{e}_\theta \qquad (3\text{-}13a)$$

where

$$E_\eta = \frac{-J_{comp}}{\sigma_a(\sinh^2\eta + \sin^2\theta)^{1/2}}\left\{\cos\theta\ \sinh\eta\left[1 - \frac{\cosh\eta_o\ Q_1'(\cosh\eta)}{Q_1(\cosh\eta_o)}\right] + \frac{\sinh^2\eta_o}{4\sinh\eta}\right\}$$

(3-13b)

and

$$E_\theta = \frac{+J_{comp}}{\sigma_a(\sinh^2\eta + \sin^2\theta)^{1/2}} \cdot \sin\theta\left[\cosh\eta - \frac{\cosh\eta_o \cdot Q_1(\cosh\eta)}{Q_1(\cosh\eta_o)}\right].$$

(3-13c)

The surface charge density $\rho_s(\theta)$ is

$$\rho_s(\theta) = \epsilon E_\eta(\eta_o, \theta) = \frac{-\epsilon J_{comp}}{\sigma_a} \cdot \frac{\sinh\eta_o\left\{\frac{1}{4} + \cos\theta\ \left[1 - C_o\right]\right\}}{(\sinh^2\eta_o + \sin^2\theta)^{1/2}}$$

(3-14)

where $C_o = \cosh\eta_o \cdot Q_1'(\cosh\eta_o)/Q_1(\cosh\eta_o) \leq -2$.

The behavior of $\rho(\theta)$ is sketched in Figures 3 and 4. For $J_{comp} > 0$, we have

$$\rho_s(\theta) < 0\ , \qquad 0 \leq \theta < \theta_N$$

$$\rho_s(\theta) > 0\ , \qquad \theta_N < \theta \leq \pi$$

(3-15)

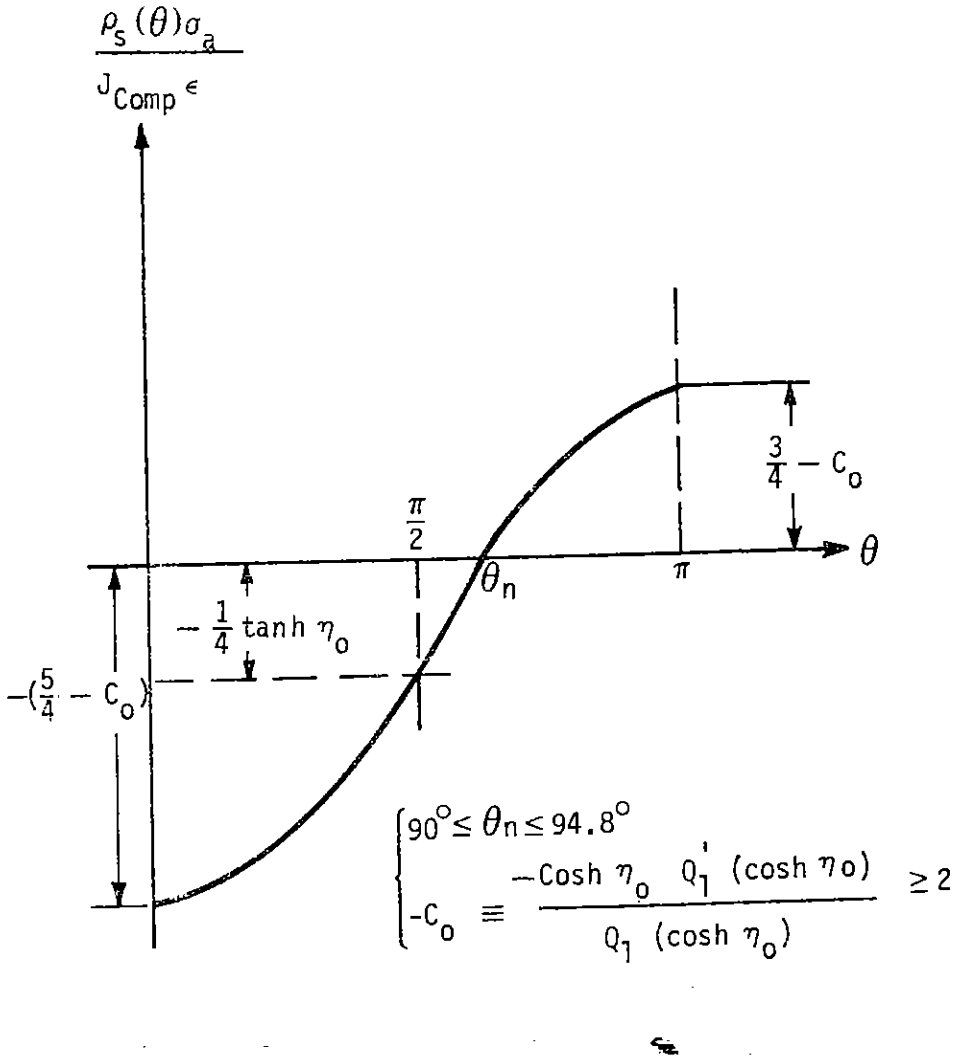

Figure 3. Surface Charge Density

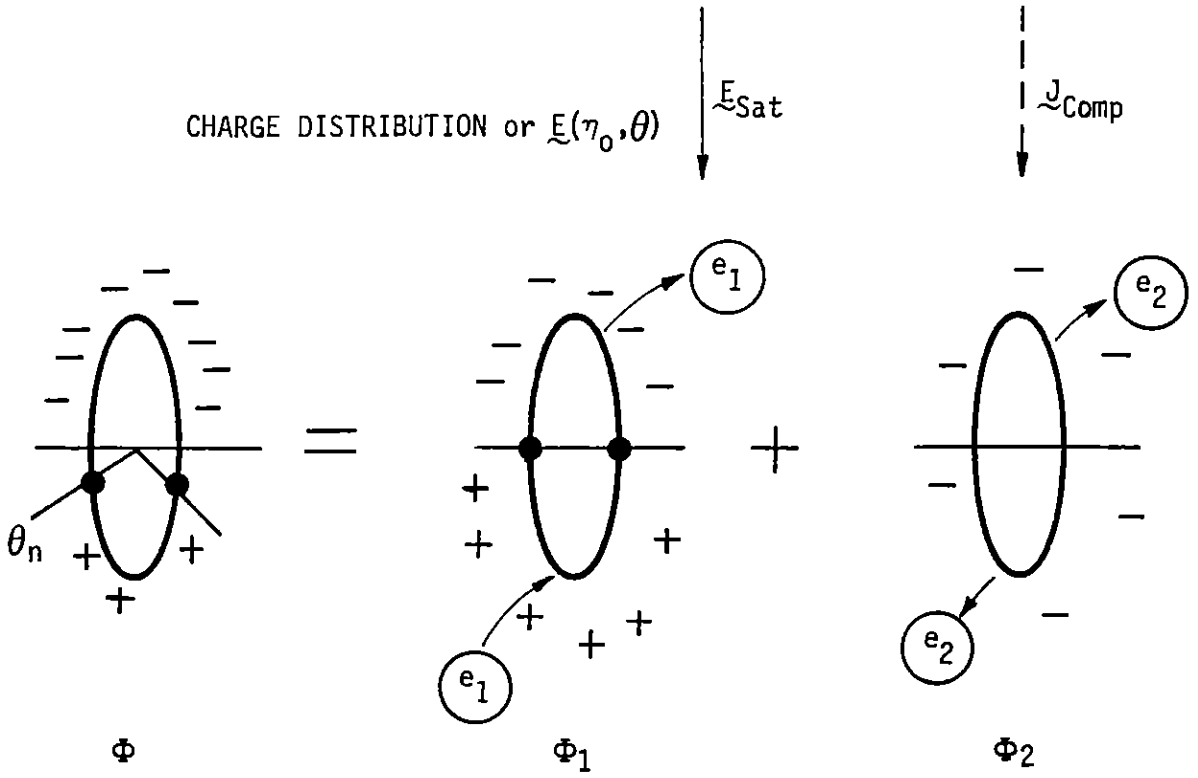

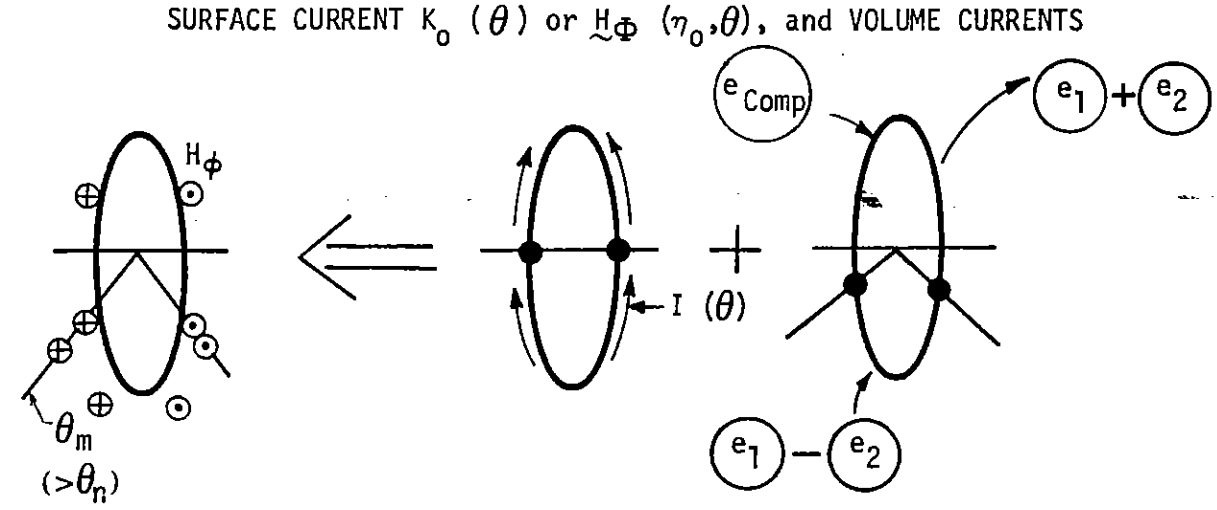

Figure 4. Charge and Current Distributions on the Prolate Spheroidal Conductor Parallel to γ- Flux.

where θ_N exists for all η_o such that

$$\begin{cases} \rho_s(\theta_N) \equiv 0, \\ \\ \theta_N = -\cos^{-1}\left\{\dfrac{\frac{1}{4}}{1 - C_o}\right\} + \pi \rightarrow 94.8^\circ \text{ if } \eta_o \rightarrow \infty \\ \qquad\qquad\qquad\qquad\quad \rightarrow 90^\circ \text{ if } \eta_o \rightarrow 0 \end{cases} \tag{3-16}$$

Thus the charge "node" $\theta = \theta_N$ lies on the prolate spheroid at $\pi/2 \leq \theta_N \leqslant 94.8^\circ$ and does not vary much with the shape of the spheroid (see Figures 3, 4, and 6).

3.2.4 The Surface Current Density $\underset{\sim}{K}$

From symmetry, $K = \underset{\sim}{e}_\theta K(\theta)$ and obeys (2-16) which now is

$$\frac{\partial}{\partial\theta}\left[\sin\theta\ K(\theta)\right] = \ell J_{comp} \sin\theta \cdot \sinh\eta_o \cdot \begin{cases} \frac{1}{4} - C_o \cos\theta, & 0 \leqslant \theta \leqslant \frac{\pi}{2} \\ \\ \frac{1}{4} + \cos\theta\left(1 - C_o\right), & \frac{\pi}{2} \leqslant \theta \leqslant \pi \end{cases} \tag{3-17}$$

and gives

$$K(\theta) = J_{comp} \cdot \ell \sinh \eta_o \cdot \begin{cases} \left(\frac{1 - \cos \theta}{4 \sin \theta} \right) \cdot \frac{\sin \theta}{2} \cdot C_o & 0 \leq \theta \leq \frac{\pi}{2} \\ \left(\frac{1 - \cos \theta - 2 \cos^2 \theta}{4 \sin \theta} \right) & \frac{\pi}{2} \leq \theta \leq \pi \end{cases} \tag{3-18}$$

Notice that $K(0) = K(\pi) = 0$, as it should, is implied by (2-16) and (2-17).

From (3-17), the total surface current

$$I(\theta) = 2\pi \ell \sinh \eta_o \sin \theta \, K(\theta) \tag{3-19}$$

clearly has a maximum at $\theta = \theta_N$ where the surface charge density $\rho(\theta_N) = 0$ and the electric field $\underset{\sim}{E}(\eta_o, \theta_N) = 0$. This is sketched in Figures 4 and 5.

3.2.5 The Surface Magnetic Field $\underset{\sim}{H}(\eta_o, \theta)$

The $\underset{\sim}{H}(\eta_o, \theta)$ is simply $\underset{\sim}{K}(\theta) \times \underset{\sim}{e}_\eta = - K(\theta) \underset{\sim}{e}_\phi$. The maximum $\underset{\sim}{H}(\eta_o, \theta)$ does not occur at θ_N where $I(\theta)$is maximum, but at $\theta = \theta_M > \theta_N$ where $I(\theta)/\sin \theta$ has a maximum because of the smaller circumference there. This is also sketched in Figures 4 and 5.

5.

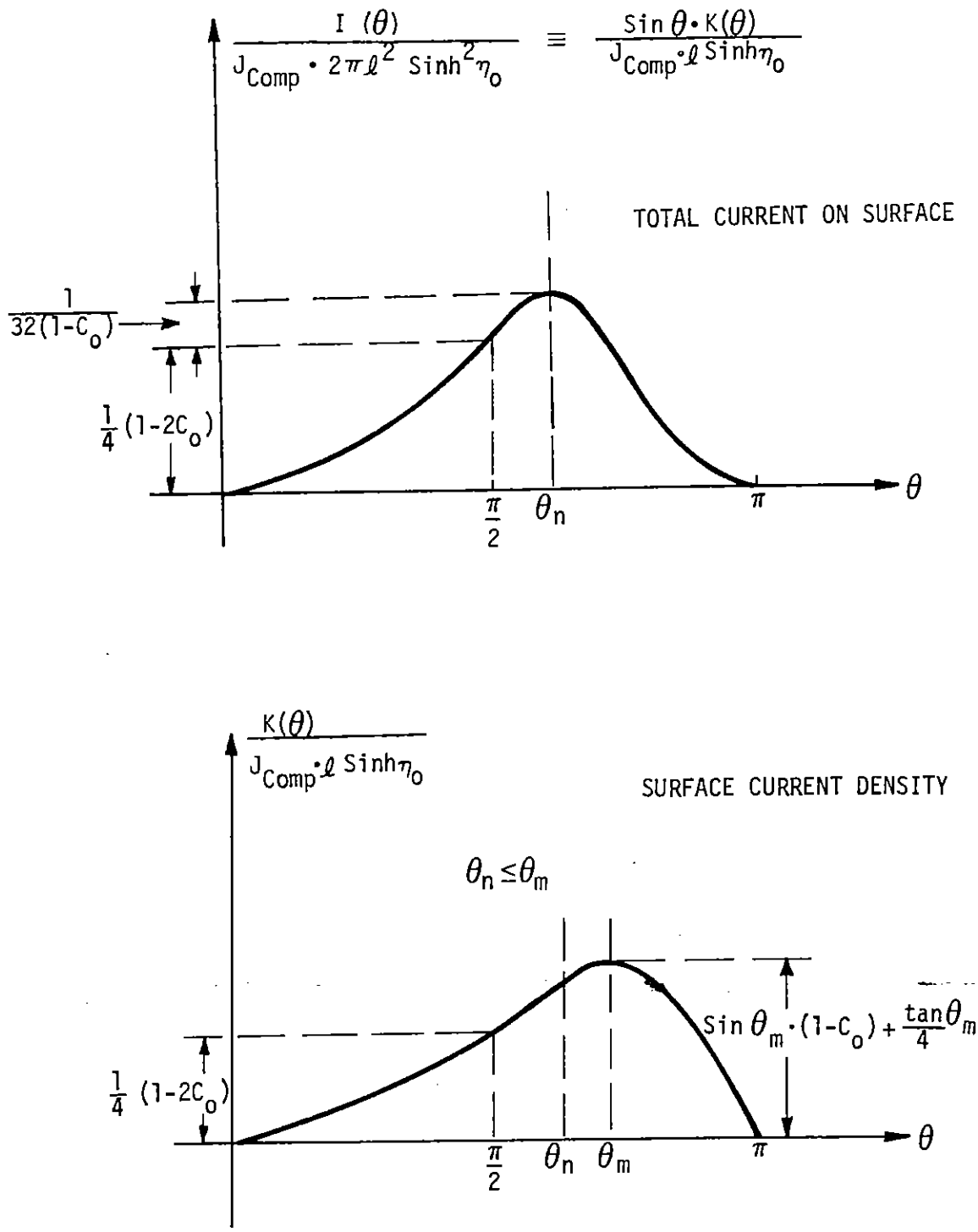

Figure 5. Total Surface Current $I(\theta)$ and Surface Current Density $K(\theta)$, where $C_o \equiv \cosh\eta_o \cdot Q_1'(\cosh\eta_o)/Q_1(\cosh\eta_o) \geq 2$.

The θ_M is a solution of

$$\begin{cases} \cos^3\theta \cdot [1 - C_o] - \cos\theta \left[\frac{3}{2} - C_o\right] - \frac{1}{2} = 0 \\ \\ \theta_N \leqslant \theta \leqslant \frac{\pi}{2} \end{cases} \tag{3-20}$$

and is very close to θ_N.

3.2.6 Remarks

From (3-14), we see that in the steady state there are always more saturation field induced charges on either half of the prolate spheroid than the total Compton current deposited net charge. Their ratio is (see Figures 3, 4, and 6):

$$\frac{q_{\text{saturation field induced, half}}}{q_{\text{deposition-total}}} = 1 - C_o \begin{cases} \xrightarrow{\eta_o \to \infty} 3, \text{ (sphere)} \\ \xrightarrow{\eta_o \to 0} \infty, \text{ (thin needle)} \end{cases} \tag{3-21}$$

where the minimum is for $\eta_o \to \infty$, i.e., the limiting case of being a sphere. Also, the peak surface current $I(\theta_N)$ is always larger than the total deposition Compton current J_{comp} A (see Figures 5 and 6):

$$\frac{I(\theta_N)}{J_{comp} \cdot \pi(\ell \sinh \eta_o)^2} = 2\left\{\frac{1}{4}(1 - 2C_o) + \frac{1}{32(1 - C_o)}\right\} \geqslant \frac{5}{2} + \frac{1}{48}. \tag{3-22a}$$

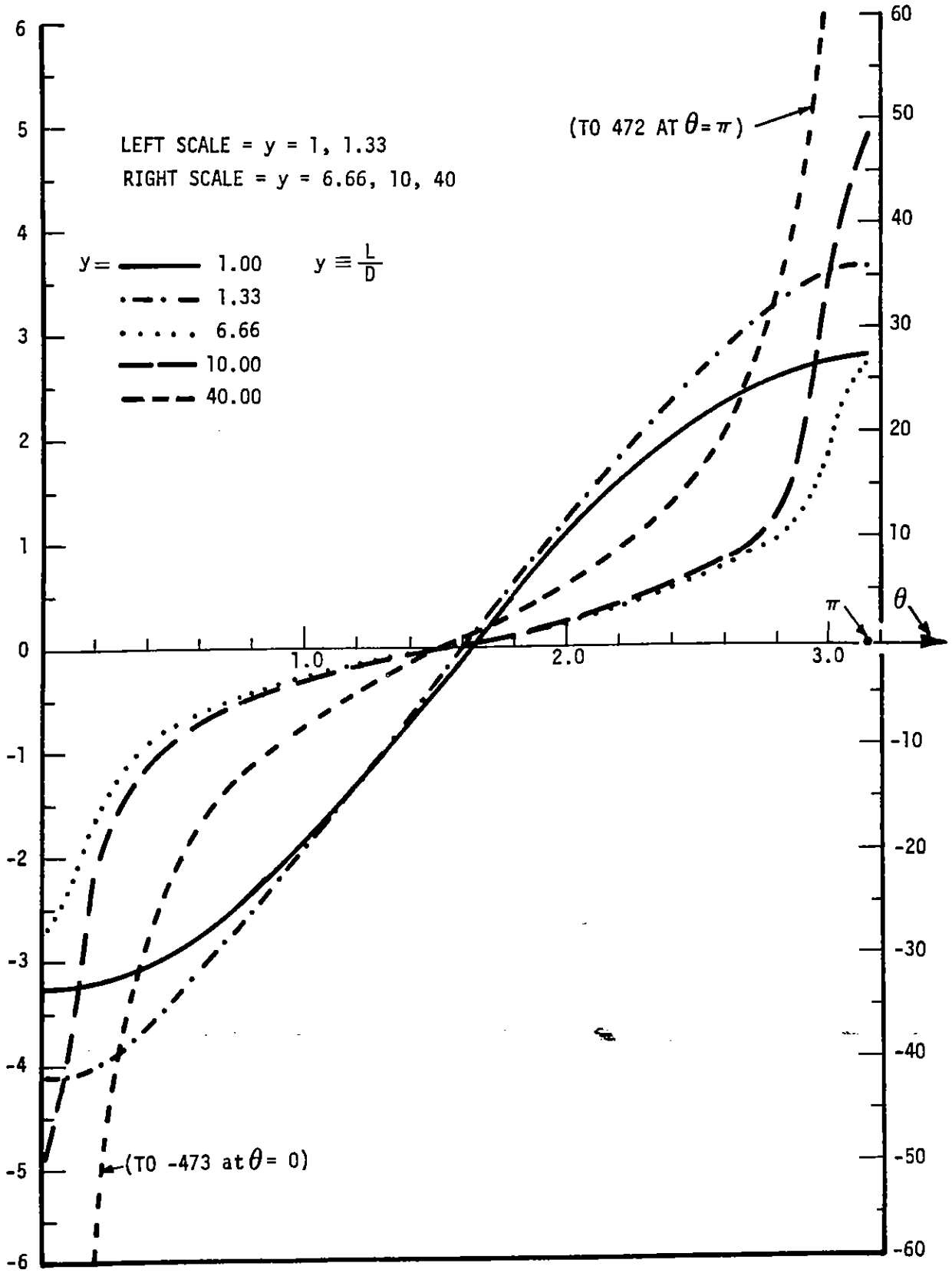

Figure 6. Plots of $E_\eta(\theta)/(J_{COMP}/\sigma_a)$ on the Surface vs θ

On the other hand, from its definition the total surface current $I(\theta)$ is

$$I(\theta) = I_1(\theta) + I_2(\theta) \tag{3-22b}$$

where $I_1(\theta) > 0$ is the backflow electron current caused by $\underset{\sim}{E}_{sat}$ and $I_2(\theta) < 0$ is the forward flow electron current caused by the direct charge deposition by J_{comp}. Therefore, we can conclude from (3-22) that the peak backflow current $I_1(\theta = \pi/2)$ $(\geq I_1(\theta_N))$ always dominates the peak Compton deposition current $|I_2(\theta = \pi/2)| \equiv |J_{comp}A/2|$ by at least a factor of 5.02. In fact, because θ_N is always near $\pi/2$, the peak I_1 is at least 6 times the peak I_2.

These results are obvious for a thin spheriod. Such a result even for a thick (almost spherical) prolate spheroid is not so obvious, but can easily be expected by reviewing the familiar spherical case which demands a charge separation three times that of a parallel plate to offset an externally applied electric field.

3.2.7 Numerical Data

Using the typical values of

$$\begin{cases} J_{comp} \sim 200 \text{ Amp/meter}^2 \\ \sigma_a \sim 2 \times 10^{-3} \text{ mho/meter} \end{cases} \qquad (3\text{-}23)$$

$$\begin{cases} D = 1.5 \text{ meter} \\ L = 10 \text{ meter} \end{cases}$$

we get the results in Table 1.

Also, we obtain various normalized numerical curves in Figure 6. Figure 6 shows the normal electrical field $E_\eta(\theta)$ on the spheroidal surface Σ, normalized with respect to the saturated immersing electric field J_{comp}/σ_a, as a function of θ for various D/L ratios. This $E/(J_{comp}/\sigma)$ is also the surface charge density normalized to the incident charge-separation surface charge density. Figure 7 shows $I(\theta)/(J_{comp} A)$, the total surface current versus θ, normalized to the intercepted Compton current, for various L/D ratios. Figures 8, 9, and 10, respectively, show the null angle θ_N, the peak surface electric field, and the peak total surface current as functions of L/D ratio.

Table 1. Typical Numerical Results for Data in (3-23).

QUANTITY	SYMBOL	VALUE
TOTAL SURFACE CHARGE	Q_{TOTAL}	1.56×10^{-7} COULOMB
PARALLEL FIELD BUILD UP TIME	$T_{BUILD-UP}$	4.43×10^{-9} SEC
CONDUCTOR POTENTIAL ABOVE INFINITY	V_{BODY}	-7.3×10^{3} VOLT
SATURATED PARALLEL ELECTRIC FIELD	E_{SAT}	10^{5} VOLT/METER
MAXIMUM ELECTRIC FIELD ON SURFACE	$E_{MAX}(0)$	2.69×10^{6} VOLT/METER (EXCEEDS BREAKDOWN VOLTAGE OF AIR AT 40 KM)
MAXIMUM SURFACE CHARGE DENSITY	ρ_{MAX}	2.38×10^{-5} COULOMB/METER^2
SURFACE CHARGE NODE	θ_N	90.54 DEGREES
MAXIMUM TOTAL CURRENT ON SURFACE	$I_{MAX}(\theta_N)$	9.06×10^{3} AMP = (25.6 X AJ_{COMP})
MAXIMUM SURFACE CURRENT DENSITY	$K_{MAX}(\theta_M)$	1.92×10^{3} AMP/METER ($\theta_M \sim 91$ DEGREES)
MAXIMUM SURFACE MAGNETIC INTENSITY	$H\phi_{-MAX}(\theta_M)$	
MAXIMUM SURFACE MAGNETIC INDUCTION	$B_{MAX}(\theta_M)$	24.2 GAUSS

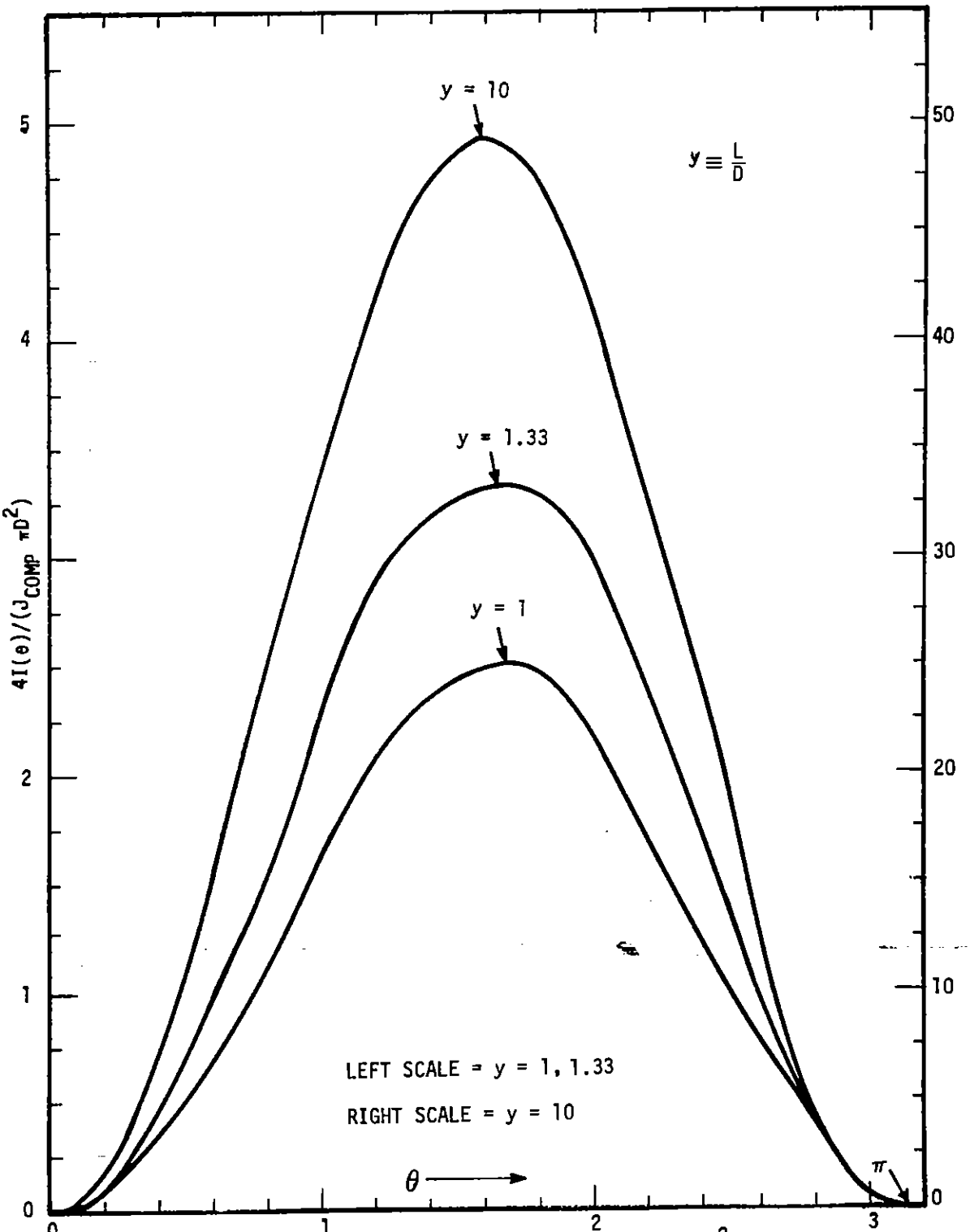

Figure 7. Plots of $4I(\theta)/(J_{COMP}\ \pi D^2)$ vs θ

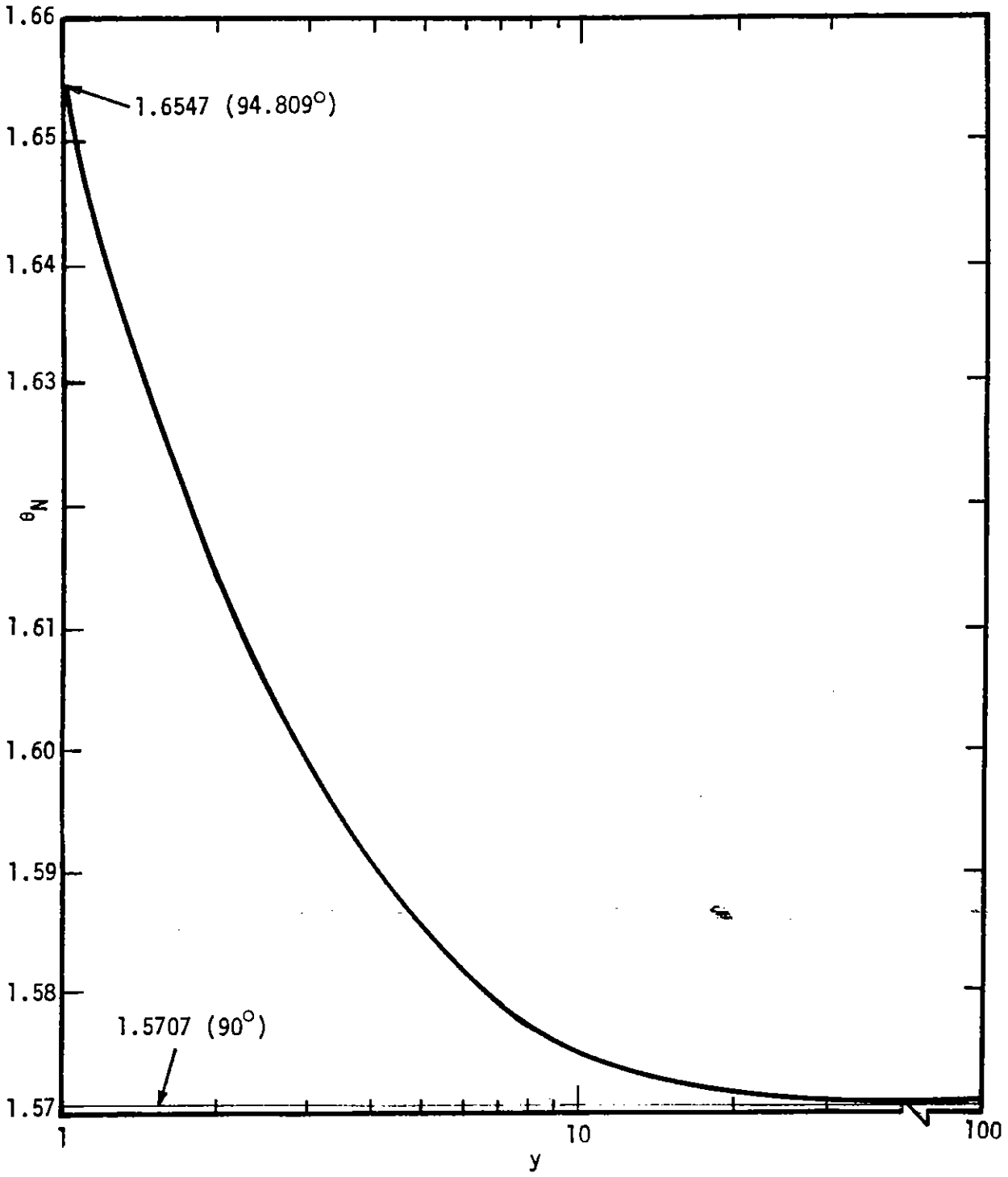

Figure 8. Plot of the Angle θ_N where E(surface) = 0 and $I(\theta_N)$ = Maximum Versus $y \equiv \frac{L}{D}$

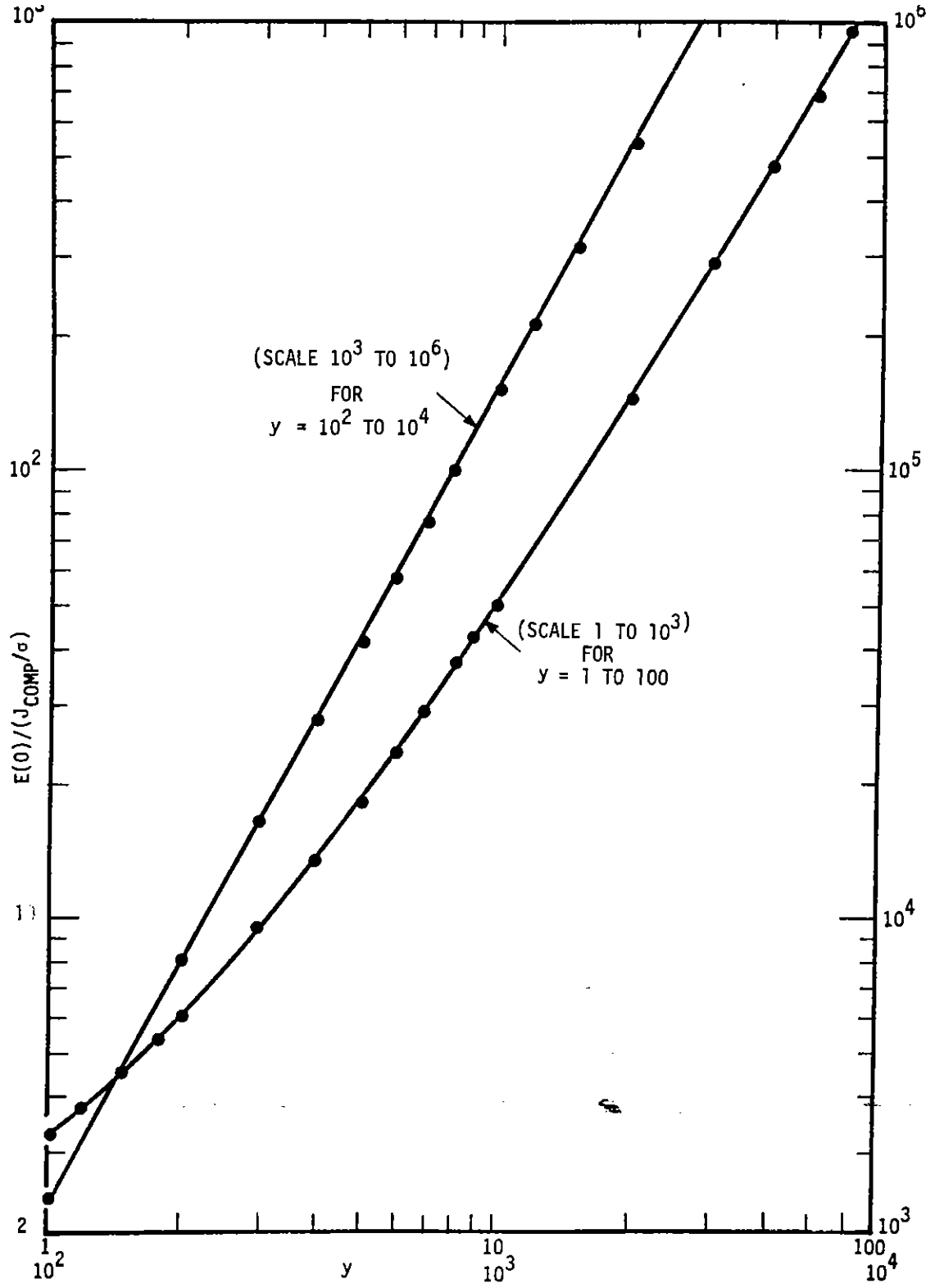

Figure 9. Plot of Peak Surface Electric Field - $E(0)/(J_{COMP}/\sigma)$ or Peak Surface Charge Density - $\rho(0)/(\epsilon J_{COMP}/\sigma)$ at $\theta=0$, Versus $y \equiv \frac{L}{D}$

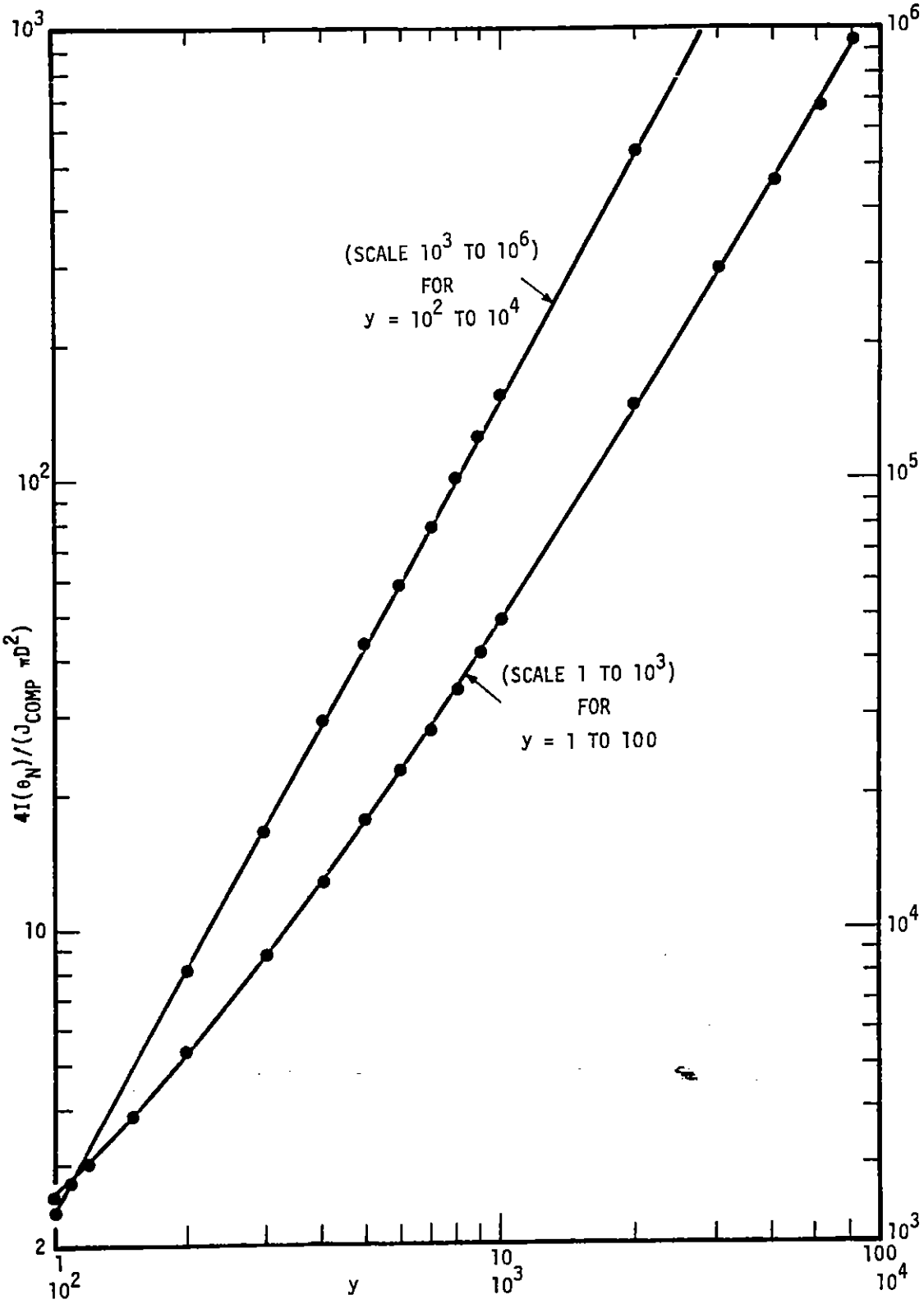

Figure 10. Plot of Peak Current $4I(\theta)/(J_{COMP}\ \pi D^2)$ at θ_N Versus $y \equiv \frac{L}{D}$

3.3 PERPENDICULAR TO γ-FLUX — A COMPARISON

Similar to Section 3.2, but with γ-flux incident along positive X-direction, we find

$$\Phi_1 = \frac{-J_{Comp}\,\ell}{\sigma_a} \sinh\eta \, \sin\theta\cos\phi \left\{ 1 - \frac{\left[Q_o(\cosh\eta) - \frac{\cosh\eta}{\sinh^2\eta} \right]}{\left[Q_o(\cosh\eta_o) - \frac{\cosh\eta_o}{\sinh^2\eta_o} \right]} \right\} \tag{3-24}$$

$$\Phi_2 = \frac{J_{comp}\,\ell\,\cosh\eta_o}{4\sigma_a} \sinh\eta_o \cdot Q_o(\cosh\eta). \tag{3-25}$$

Here we want to compare the effect of the parallel E_{sat} to that of the charge depositing J_{comp} by examining the ratio

$$\frac{q_{\text{parallel induced, half spheroid}}}{q_{total}} = \frac{2}{\cosh\eta_o \left\{ \cosh\eta_o - \frac{1}{2}\sinh^2\eta_o \; n\left[\frac{\cosh\eta_o + 1}{\cosh\eta_o - 1} \right] \right\}} \longrightarrow \begin{matrix} 3, \; \eta_o \to \infty \\ 2, \; \eta_o \to 0 \end{matrix} \tag{3-26}$$

as was done in (3-21) for the parallel induced case. From (3-26) and (3-21), we conclude that for the prolate spheriodal conductor of any shape and orientation, the backflow current caused by the parallel charge-separation electric field always dominates that caused by direct charge deposition.

SECTION 4

REMARKS AND SUMMARY

4.1 EXTENSION TO TIME-DEPENDENT PROBLEM

Conceptually, the time-dependent problem is quite similar to the steady-state one. First, without the conductor's presence at all, we have $\underset{\sim}{J}_{\text{driving}}(\underset{\sim}{X}, t)$, $\sigma(\underset{\sim}{X}, t)$, and $\underset{\sim}{E}^{\text{in}}(\underset{\sim}{X}, t)$ and $\underset{\sim}{B}^{\text{in}}(\underset{\sim}{X}, t)$ (= 0 if symmetry dictates so) all produced by the γ-rays in the environment (air and other surrounding materials). Second, the presence of the conductor introduces

$$\underset{\sim}{E}^{sc} = \underset{\sim}{E}_1^{sc} + \underset{\sim}{E}_2^{sc} \tag{4-1a}$$

$$\underset{\sim}{H}^{sc} = \underset{\sim}{H}_1^{sc} + \underset{\sim}{E}_2^{sc} \tag{4-1b}$$

$$\underset{\sim}{J}^{sc} = -\underset{\sim}{J}_{\text{driving}}(\underset{\sim}{X}, t) \cdot U(\underset{\sim}{X} - \underset{\sim}{X}_{\text{shadow \& body}}). \tag{4-1c}$$

Here, the $\underset{\sim}{J}^{sc}$ is the geometrical shadow current that is caused by the γ-thickness of the conductor and the step function $\underset{\sim}{U}(\underset{\sim}{X} - \underset{\sim}{X}_{SB}) = 1$, 0 if $X \epsilon V$, $V_S + V_{\text{body}}$, respectively. The $\underset{\sim}{E}_2^{sc}$ and $\underset{\sim}{H}_2^{sc}$ are the fields caused by $\underset{\sim}{J}^{sc}$, without any boundary condition imposed, in the medium with μ, ϵ, $\sigma(\underset{\sim}{X}, t)$. Then the $\underset{\sim}{E}_1^{sc}$ and $\underset{\sim}{H}_1^{sc}$ are fields that satisfy the homogeneous field equations in the volume $V + V_S$ and the inhomogeneous boundary condition on Σ such that

$$\underset{\sim}{n} \times \underset{\sim}{E}_1^{sc} = -\underset{\sim}{n} \times (\underset{\sim}{E}^{\text{in}} + \underset{\sim}{E}_2^{sc}) \text{ on } \Sigma \tag{4-2}$$

and radiation condition at Σ_∞(it therefore must have a singularity in V_{body}). Notice that if a plane γ-flux $F_\gamma = F_\gamma\ (t - z/c)$ is considered, the $J_{driving}(\underset{\sim}{X},t)$, $\underset{\sim}{J}^{sc}(\underset{\sim}{X}, t)$, $\underset{\sim}{E}^{in}\ (\underset{\sim}{X}, t)$, $\underset{\sim}{H}^{in}\ (\underset{\sim}{X}, t)$ can be easily obtained, with the $\sigma(\underset{\sim}{X}, t)$ fully taken into account for the $\underset{\sim}{E}^{in}\ (\underset{\sim}{X}, t)$. But the $\underset{\sim}{E}_2^{sc}$, caused by the simple $\underset{\sim}{J}^{sc}$, is difficult to obtain analytically if the full $\sigma(\underset{\sim}{X}, t)$ is used for the medium. Even more difficult to get analytically is the $\underset{\sim}{E}_1^{sc}$, with the geometrical shape of Σ further complicating the process.

Thus for time-dependent problems, we need special analytical techniques and justified approximations to simplify and/or decouple the problem. But if we are only interested in quantities on the conductor's surface Σ, we are askihg for considerably less than the whole field, and some simplification may be used. A time-dependent solution for the prolate spheroid will be presented in a separate report.

4.2 SUMMARY

In this work, we have formulated and clearly analyzed the EMP source region problem for a conductor immersed there and in steady state. We analytically solved for the case of a prolate spheriodal conductor, found that the backflow of field-induced fields and currents are always greater than those effects of the direct Compton charge deposition, and plotted the results. The steady analysis is directly applicable to the case of long γ-duration, small conductor, and slowly varying air conductivity. It also provides a clear way of analyzing the time-dependent problem and probably gives the upper limit when the incident field is rising for those frequencies whose skin depth in air is much larger than the conductor's dimensions.

REFERENCES

1. W.J. Karzas and R. Latter, Phy. Rev., 126, #6, 1919 (June 1962), 137, #5B, B1369 (March, 1965), also J. Geoph. Research, 67, #12, 4635, (November 1962).

2. R. Latter and R.E. LeLevier, J. Geoph. Research, 68, #6, 1643 (March 1963)

3. C.L. Longmire, Theory of the EMP from Nuclear Surface Burst, Report LANC-R-6, Los Alamos Nuclear Corporation (1970).

4. C.E. Baum (ed.), EMP Interaction Notes, AFWL (see for many interesting papers).

5. C.T.C. Mo., The Numerical Code Rondine and Analysis, next report in this DNA Quarterly Report, RDA-TR-5900-002 (June 1974).

6. R. Evans, The Atomic Nucleus, McGraw-Hill (1955).

7. W.J. Karzas and R. Latter, op. cit.

8. C.E. Baum, op. cit., #2, 6, and 12.

9. R.Evans, op. cit., Chapter 18.

10. C.L. Longmire, op. cit.

11. M.J. Berger and S.M. Seltzer, Tables of Energy Losses and Ranges of Elections and Positions, NASA SP-3012 (1964).

12. C.L. Longmire, op. cit., C.E. Baum, op. cit., also W.J. Karzas, R. Latter, RM-3671-PR, Rand Corporation (May 1963).

13. W.J. Karzas and R. Latter, op. cit., and also

$$\int_0^\infty d(at)\ \frac{e^{at}}{1+e^{\frac{3at}{2}}} = \int_1^\infty \frac{dx}{1+x^{\frac{3}{2}}}$$

$$= 2\left\{\frac{\ell n 4}{6} + \frac{1}{\sqrt{3}}\left[\frac{\pi}{2} - \tan^{-1}\frac{1}{\sqrt{3}}\right]\right\} = 1.66$$

14. C.L. Longmire, op. cit.

15. The influence of the conductor's field on the driving Compton current is completely ignored in this work.

16. When $B \equiv 0$, assuming an average collision time τ gives

$$\frac{m\underset{\sim}{v}}{\tau} = eE$$

and

$$\underset{\sim}{J} = ne\underset{\sim}{v} = \frac{ne^2\tau}{m}\underset{\sim}{E} \equiv \sigma\underset{\sim}{E}$$

Now when $B \neq 0$, still assuming the same τ gives

$$\frac{m\underset{\sim}{v}}{\tau} = e(\underset{\sim}{E} + \underset{\sim}{v} \times \underset{\sim}{B})$$

which yields (2-13) by solving v in terms of the fields.

17. To depict it, one can think:

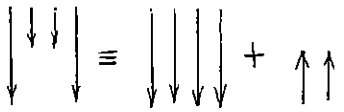

for the volume current.

18. See any vector analysis table on curvilinear coordinates, e.g., Ref. 19.

19. P. Moon and D.E. Spencer, Field Theory Handbook, Springer Verlag (1961).

20. Notice that

$$\underset{\sim}{e}_z = \left[\underset{\sim}{e}_\eta \sinh \eta \cos \theta - \underset{\sim}{e}_\theta \cosh \eta \sin \theta\right] \cdot \frac{1}{\sqrt{\sinh^2\eta + \sin^2\theta}}$$